Journal of Steroid Biochemistry & Molecular Biology 165 (2017) 268–276

Contents lists available at ScienceDirect

Journal of Steroid Biochemistry & Molecular Biology

journal homepage: www.elsevier.com/locate/jsbmb

Fluorinated oxysterol analogues: Synthesis, molecular modelling and LXRβ activity

Cristian R. Rodriguez[a], Lautaro D. Alvarez[a,1], M.Virginia Dansey[a,1], Luciano S. Paolo[b], Adriana S. Veleiro[a], Adali Pecci[b], Gerardo Burton[a,*]

[a] Universidad de Buenos Aires, CONICET. UMYMFOR and Departamento de Química Orgánica, Facultad de Ciencias Exactas y Naturales, Pabellón 2, Ciudad Universitaria, C1428EGA Buenos Aires, Argentina
[b] Universidad de Buenos Aires, CONICET. IFIBYNE and Departamento de Química Biológica, Facultad de Ciencias Exactas y Naturales, Pabellón 2, Ciudad Universitaria, C1428EGA Buenos Aires, Argentina

ARTICLE INFO

Article history:
Received 12 April 2016
Received in revised form 19 June 2016
Accepted 4 July 2016
Available online 22 July 2016

Keywords:
Oxysterols
Cholestenoic acid
Liver X receptor
Molecular dynamics

ABSTRACT

Liver X receptors (LXRs) are nuclear receptors that play central roles in the transcriptional control of lipid metabolism. The ability of LXRs to integrate metabolic and inflammation signalling makes them attractive targets for intervention in human metabolic diseases. Several oxidized metabolites of cholesterol (oxysterols) are endogenous LXR ligands, that modulate their transcriptional responses. While 25*R*-cholestenoic acid is an agonist of the LXRs, the synthetic analogue 27-norcholestenoic acid that lacks the 25-methyl is an inverse agonist. This change in the activity profile is triggered by a disruption of a key interaction between residues His435 and Trp457 that destabilizes the H11-H12 region of the receptor and favors the binding of corepressors. The introduction of fluorine atoms on the oxysterol side chain can favor both hydrophobic interactions as well as hydrogen bonds with the fluorine atoms and may thus induce changes in the receptor that may lead to changes in the activity profile. To evaluate these effects we have synthesized two fluorinated 27-nor-steroids, analogues of 27-norcholestenoic acid, the 25,25-difluoroacid and the corresponding 26-alcohol. The key step was a Reformatsky reaction on the C-24 cholenaldehyde, with ethyl bromodifluoroacetate under high intensity ultrasound (HIU) irradiation, followed by a Barton-McCombie type deoxygenation. Activity was evaluated in a luciferase reporter assay in the human HEK293 T cells co-transfected with full length human LXRβ expression vector. The 25,25-difluoro-27-norcholestenoic acid was an inverse agonist and antagonist similar to its non-fluorinated analogue while its reduced derivative 25,25-difluoro-27-norcholest-5-ene-3β,26-diol was an agonist. Molecular dynamics simulation of the ligand-receptor complexes showed that the difluoroacid disrupted the His435-Trp457 interaction although the resulting conformational changes were different from those induced by the non-fluorinated analogue. In the case of the difluoroalcohol, the fluorine atoms actively participated in the interaction with several residues in the ligand binding pocket leading to a stabilization of the active receptor conformation.

1. Introduction

Oxysterols, the oxygenated metabolites of cholesterol, not only form part of the cholesterol degradation pathway, but they also are regulatory molecules with diverse specific biological actions. Particularly, they act as endogenous modulators of the Nuclear Receptor (NR) superfamily transcription factors, involved in essential functions of cellular physiology. As part of the extrahepatic alternative pathway of bile acid synthesis, CYP27A1, one of the ubiquitous P450 enzymes, produces two oxygenated steroids at C-27, 25*R*-cholestenoic acid (**1**) and 26-hydroxycholesterol (**2**) (Fig. 1), that bind to the Liver X Receptors (LXRs) and modulate their transcriptional responses [1,2].

In the last two decades, LXRs have emerged as attractive pharmacological targets due to their relevant abilities to regulate lipid metabolism and cholesterol transport, as well as glucose homeostasis and inflammatory response [3]. Two LXR isoforms

* Corresponding author.
E-mail address: burton@qo.fcen.uba.ar (G. Burton).
[1] These authors contributed equally to this work.

http://dx.doi.org/10.1016/j.jsbmb.2016.07.001
0960-0760/

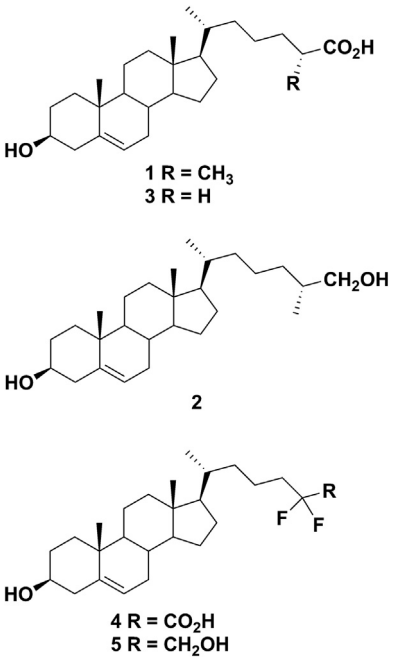

Fig. 1. Endogenous and synthetic LXR ligands.

have been described (LXRα and LXRβ) that form heterodimers with the retinoid X receptor (RXR). Structurally, LXRs are modular proteins organized into three domains: a N-terminal activation domain that recruits ligand-independent co-activators, a central DNA-binding domain and a C-terminal ligand binding domain (LBD), which also is involved in the binding of cofactors at the AF-2 region. Upon the binding of agonist ligands, the LXR-LBD undergoes conformational modifications that result in the release of corepressors and recruitment of coactivators, leading to gene expression regulation. There is evidence that LXR agonists might be useful for the treatment of Alzheimer's disease and other neurodegenerative diseases of the CNS [4], on the other hand the undesirable effect of LXR agonists on hepatic lipogenesis has prompted the development and characterization of LXR antagonists and inverse agonists [5,6].

Recently, in the search for novel oxysterol analogues with simplified steroid side chains, we synthesized the 27-nor-steroid **3**, analogue of compound **1** (Fig. 1) [7]. Surprisingly, we found that compound **3** behaved as an inverse LXR agonist with an improved capacity of the LXRβ/**3** complex to bind corepressors rather than coactivators. Even more, *in silico* MD simulations revealed that the absence of the C-25 methyl provokes a disruption of the His435-Trp457 interaction, and consequently a destabilization of the H11-H12 region of the receptor.

Based on these results and considering that replacing hydrogen by fluorine entails a large electronic effect on neighboring functional groups, thus increasing the acidity of carboxylic acids and alcohols, we have now prepared two fluorinated 27-nor-steroids compounds **4** and **5**. These are analogues of **3**, in which polarity and lipophicility of the side chain have changed. We wondered if the increased acidity of the terminal group at C-26 could have an effect on the interaction with the LXRs, but also if the fluorine atoms at C-25 could interact *per se* with residues in the LXR ligand binding pocket (e.g. His435), as observed in the crystal structure of LXR complexes with the non-steroidal ligand GW3965 (pdb:1pq6, pdb:3ipq and pdb:4nqa).

2. Materials and methods

2.1. Chemistry

Mps were taken on a Fisher-Johns apparatus and are uncorrected. NMR spectra were recorded on an Avance II 500 NMR spectrometer (^{1}H at 500.13 MHz, ^{19}F 470,59 MHz, ^{13}C at 125.77 MHz). Chemical shifts are given in ppm downfield from TMS as internal standard (^{1}H and ^{13}C) or $CFCl_3$ external standard (^{19}F), J values are given in Hz. Multiplicity determinations and 2D spectra (COSY, NOESY, HSQC and HMBC) were obtained using standard Bruker software. Exact mass spectra were obtained using a Bruker micrOTOF-Q II mass spectrometer, equipped with an ESI source operating in positive mode. Flash chromatography was carried out on silica gel 60, 0.0040-0.0063 mm, Merck 9385. High intensity ultrasound (HIU) irradiation was provided by an ultrasonic processor probe system SonicCell VCX 750 (20 KHz, 750 W, 3 mm stepped tip at power level of 20–30%) in a reactor from Sonics and Materials. Medium Pressure Liquid Chromatography (MLPC) was carried out on a Buchi Sepacore purification system C-615 equipped with two pumps of 10 bar maximum pressure. Thin layer chromatography (tlc) analysis was performed on silica gel 60 F254 (0.2 mm thick). The homogeneity of all compounds was confirmed by tlc and ^{1}H NMR. Solvents were evaporated at reduced pressure and *ca.* 40–50 °C. 3β-(*t*-Butyldimethylsilyloxy)-chol-5-en-24-al (**6**) was prepared following the procedure previously described by us [7].

2.1.1. 3β-(t-Butyldimethylsilyloxy)-25,25-difluoro-24ξ-hydroxy-27-norcholest-5-en-26-oic acid ethyl ester (7)

To a solution of aldehyde **6** (363 mg, 0.770 mmol) in THF (2.7 mL), activated Zn dust (151 mg, 2.30 mmol) and iodine (58.4 mg, 0.230 mmol) were added and Ar was bubbled through the mixture. The mixture was sonicated 1 cycle, and ethyl α-bromo-α,α-difluoroacetate (468 mg, 2.30 mmol) was added, followed by THF (1 mL). The reaction mixture was sonicated for 10 min in (6 × 4) s pulse mode. During irradiation, the reaction vessel was immersed in a circulating water bath at 25 °C. At the end of the reaction period, the reaction mixture was poured onto an aqueous saturated solution of NH_4Cl (10 mL), extracted with ethyl acetate (3 × 10 mL), washed with aqueous NaCl, and the solvent evaporated. The resulting solid was purified by MPLC (flow rate: 10 mL/min, hexane-ethyl acetate 97:3) to give **7** as a 1:1 mixture of epimers at C-24 (298 mg, 65.0%). ^{1}H NMR (500.13 MHz, $CDCl_3$) δ_H: 5.31 (1H, m, H-6); 4.36 (2H, q, *J* = 7.0 Hz, O-C**H**$_2$CH$_3$); 3.98 (1H, m, H-24 epimer 1); 3.94 (1H, m, H-24 epimer 2); 3.48 (1H, tt, 11.1 and 5.4 Hz, H-3); 2.27 (1H, m, H-4β); 2.17 (1H, m, H-4α); 2.03 (1H, m, H-23a epimer 1); 2.00 (1H, m, H-12β); 1.97 (1H, m, H-7β); 1.83 (1H, m, H-16α); 1.80 (1H, m, H-1β); 1.78 (1H, m, H-23a epimer 2); 1.74 (1H, m, H-22a epimer 1), 1.73 (1H, m, H-2α); 1.59 (1H, m, H-15β); 1.58 (1H, m, H-23b epimer 1); 1.55 (1H, m, H-2β); 1.54 (1H, m, H-7α); 1.50 (1H, m, H-22b); 1.47 (2H, m, H-11); 1.46 (1H, m, H-20 epimer 1); 1.45 (1H, m, H-20 epimer 2); 1.44 (1H, m, H-8); 1.39 (1H, m, H-23b epimer 2); 1.37 (2H, t, *J* = 7.0 Hz, O-CH$_2$C**H**$_3$); 1.33 (1H, m, H-22b); 1.27 (1H, m, H-16β); 1.16 (1H, m, H-12α); 1.11 (1H, m, H-17); 1.10 (1H, m, H-22a epimer 2); 1.08 (1H, m, H-15α); 1.03 (1H, m, H-1α); 1.00 (3H, s, H-19); 0.99 (1H, m, H-14); 0.95-0.94 (3H, d, *J* = 6.5 Hz, H-21); 0.91 (1H, m, H-9); 0.89 (9H, s, $(CH_3)_3$C-Si); 0.682 (3H, s, H-18 epimer 2); 0.677 (3H, s, H-18 epimer 1); 0.06 (6H, s, $(CH_3)_2$-Si); ^{13}C NMR (125.77 MHz, $CDCl_3$) δ_C: 163.7 (t, *J* = 31.0 Hz, C-26); 141.6 (C-5); 121.1 (C-6); 114.6 (t, *J* = 254 Hz, C-25); 72.6 (C-3); 72.6 (t, *J* = 26.2 Hz-C-24 epimer 1); 72.0 (t, *J* = 25.2 Hz, C-24 epimer 2); 63.0 (O-**C**H$_2$CH$_3$); 56.75 and 56.73 (C-14); 55.76 and 55.70 (C-17); 50.2 (C-9); 42.8 (C-4); 42.35 and 42.34 (C-13); 39.8 (C-12); 37.4 (C-1); 36.6 (C-10); 35.7 and 35.2 (C-20); 32.1 (C-2); 31.9 (C-7 and C-8); 31.6 and 31.2 (C-22); 28.2 and 28.1 (C-16); 26.0 and 25.6 (C-23);

25.9 (($\mathbf{C}H_3)_3$C-Si); 24.2 (C-15); 21.0 (C-11); 19.4 (C-19); 18.6 and 18.4 (C-21); 18.3 (($CH_3)_3\mathbf{C}$-Si); 14.0 (O-$CH_2\mathbf{C}H_3$); 11.86-11.85 (C-18); −4.60 (($CH_3)_2$-Si); ^{19}F NMR (470.59 MHz, $CDCl_3$) δ_F: −114.46 (dd, J_{FF} = 263 Hz, J_{FH} = 3.5 Hz, F-25a epimer 1); −115.01 (dd, J_{FF} = 262 Hz, J_{FH} = 3.5 Hz, F-25a epimer 2); −122.30 (dd, J_{FF} = 264 Hz, J_{FH} = 14.7 Hz, F-25b epimer 1); −122.54 (dd, J_{FF} = 264 Hz, J_{FH} = 15.2 Hz, F-25b epimer 2); HRMS-ESI: calculated for $C_{34}H_{58}F_2NaO_4Si$: 619.3965, found 619.3972.

2.1.2. 3β-(t-Butyldimethylsilyloxy)-25,25-difluoro-27-norcholest-5-en-26-oic acid ethyl ester (8)

To a solution of compound **7** (50.0 mg, 0.08 mmol) in dry 1,2-dichloroethane (5.0 mL), thiocarbonyldiimidazole (37.3 mg, 0.2 mmol) and dimethylaminopyridine (0.5 mg, 0.004 mmol) were added. The mixture was heated under reflux for 3 h, allowed to cool to room temperature and the solvent evaporated. Purification by MPLC (Flow rate: 10 mL/min; hexane-ethyl acetate 97:3 → 90:10) gave the thionocarbonate as an amorphous solid (54.2 mg, 91.0%).

A solution of the thionocarbonate (54.2 mmol, 0.08 mmol) obtained above in dry toluene (2.2 mL) was brought to boiling under Ar, and diphenylsilane (42.7 μL, 0.23 mmol) added. The reaction mixture was subsequently treated with 122 μL portions of a solution of lauroyl peroxide in toluene (0.112 g/mL) at 20 min intervals during 3 h. When the reaction was complete (tlc) the solvent was evaporated in vacuum and the residue purified by MPLC (flow rate: 10 mL/min; hexane-ethyl acetate 100 → 99:1) to give compound **8** as an amorphous solid (35.7 mg, 80.0%). ^{1}H NMR (500.13 MHz, $CDCl_3$) δ_H: 5.32 (1H, dt, J = 5.0 and 1.9 Hz, H-6); 4.33 (2H, q, J = 7.0 Hz, O-C$\mathbf{H}_2$CH$_3$); 3.48 (1H, tt, 10.7 and 5.2 Hz, H-3); 2.27 (1H, m, H-4β); 2.17 (1H, m, H-4α); 2.01 (2H, m, H-24); 2.00 (1H, m, H-12β); 1.97 (1H, m, H-7β); 1.82 (1H, m, H-16α); 1.81 (1H, m, H-1β); 1.72 (1H, m, H-2α); 1.59 (1H, m, H-15β); 1.54 (2H, m, H-23a and H-2β); 1.52 (1H, m, H-7α); 1.48 (2H, m, H-11); 1.44 (1H, m, H-8); 1.40 (1H, m, H-20); 1.36 (2H, t, J = 7.0 Hz, O-CH$_2$C$\mathbf{H}_3$); 1.35 (1H, m, H-23b); 1.25 (1H, m, H-16β); 1.16 (1H, m, H-12α); 1.10 (3H, m, H-17 and H-22); 1.08 (1H, m, H-15α); 1.05 (1H, m, H-1α); 1.00 (3H, s, H-19); 0.99 (1H, m, H-14); 0.93 (3H, d, J = 6.0 Hz, H-21); 0.92 (1H, m, H-9); 0.89 (9H, s, $(CH_3)_3$C-Si); 0.68 (3H, s, H-18); 0.06 (6H, s, $(CH_3)_2$-Si); ^{13}C NMR (125.77 MHz, $CDCl_3$) δ_C: 164.5 (t, J = 33.1 Hz, C-26); 141.6 (C-5); 121.1 (C-6); 116.4 (t, J = 250 Hz, C-25); 72.6 (C-3); 62.7 (O-$\mathbf{C}H_2CH_3$); 56.8 (C-14); 55.8 (C-17); 50.2 (C-9); 42.8 (C-4); 42.3 (C-13); 39.8 (C-12); 37.4 (C-1); 36.6 (C-10); 35.5 (C-20); 35.4 (C-22); 34.9 (t, J = 23.0, C-24); 32.1 (C-2); 31.91 (C-7); 31.89 (C-8); 28.2 (C-16); 25.9 (($\mathbf{C}H_3)_3$C-Si); 24.2 (C-15); 21.0 (C-11); 19.4 (C-19); 18.5 (C-21); 18.3 (($CH_3)_3\mathbf{C}$-Si); 18.0 (t, J = 4.2, C-23); 14.0 (O-$CH_2\mathbf{C}H_3$); 11.8 (C-18); −4.60 (($CH_3)_2$-Si); ^{19}F NMR (470.59 MHz, $CDCl_3$) δ_F: −105.51 (ddd, J_{FF} = 259 Hz, J_{FH} = 17.9 Hz and 16.0 Hz, F-25a); −106.19 (ddd, J_{FF} = 259 Hz, J_{FH} = 17.9 Hz and 16.0 Hz, F-25b); HRMS-ESI: calculated for $C_{34}H_{58}F_2NaO_3Si$: 603.4015, found 603.4016.

2.1.3. 25,25-Difluoro-3β-hydroxy-27-norcholest-5-en-26-oic acid ethyl ester (9)

To a solution of **8** (40.0 mg, 0.06 mmol) in THF (1 mL) and acetonitrile (1 mL) cooled to 0 °C, was added 40% hydrofluoric acid (0.05 mL) and the solution stirred at 25 °C for 2 h. The reaction mixture was neutralized with aqueous potassium bicarbonate and extracted with ethyl acetate. The organic layer was washed with water, dried with sodium sulphate and the solvent evaporated. Purification by MPLC (flow rate: 5 mL/min; hexane-ethyl acetate 95:5 → 90:10) gave compound **9** as an amorphous solid (33.0 mg, 95%). ^{1}H NMR (500.13 MHz, $CDCl_3$) δ_H: 5.35 (1H, dt, J = 5.5 and 1.9 Hz, H-6); 4.33 (2H, q, J = 7.0 Hz, O-C$\mathbf{H}_2$CH$_3$); 3.53 (1H, tt, 10.6 and 4.9 Hz, H-3); 2.30 (1H, ddd, J = 12.9, 5.0 and 2.0 Hz, H-4β); 2.23 (1H, m, H-4α); 2.00 (3H, m, H-12β and H-24); 1.97 (1H, m, H-7β); 1.81 (1H, m, H-16α); 1.85 (1H, m, H-1β); 1.84 (1H, m, H-2α); 1.59 (1H, m, H-15β); 1.54 (1H, m, H-23a); 1.50 (1H, m, H-2β); 1.52 (1H, m, H-7α); 1.48 (2H, m, H-11); 1.46 (1H, m, H-8); 1.40 (1H, m, H-20); 1.35 (2H, t, J = 7.0 Hz, O-CH$_2$C$\mathbf{H}_3$); 1.35 (1H, m, H-23b); 1.25 (1H, m, H-16β); 1.16 (1H, m, H-12α); 1.09 (1H, m, H-17); 1.10 (2H, m, H-22); 1.07 (1H, m, H-15α); 1.08 (1H, m, H-1α); 1.00 (3H, s, H-19); 0.98 (1H, m, H-14); 0.92 (3H, d, J = 6.5 Hz, H-21); 0.93 (1H, m, H-9); 0.68 (3H, s, H-18); ^{13}C NMR (125.77 MHz, $CDCl_3$) δ_C: 164.5 (t, J = 32.7 Hz, C-26); 140.8 (C-5); 121.7 (C-6); 116.4 (t, J = 250 Hz, C-25); 71.8 (C-3); 62.7 (O-$\mathbf{C}H_2CH_3$); 56.7 (C-14); 55.8 (C-17); 50.1 (C-9); 42.34 (C-4); 42.28 (C-13); 39.7 (C-12); 37.2 (C-1); 36.5 (C-10); 35.5 (C-20); 35.4 (C-22); 34.9 (t, J = 22.6, C-24); 31.9 (C-7 and C-8); 31.7 (C-2); 28.2 (C-16); 24.2 (C-15); 21.1 (C-11); 19.4 (C-19); 18.5 (C-21); 18.0 (t, J = 4.0, C-23); 14.0 (O-$CH_2\mathbf{C}H_3$); 11.8 (C-18); ^{19}F NMR (470.59 MHz, $CDCl_3$) δ_F: −105.49 (ddd, J_{FF} = 258 Hz, J_{FH} = 17.4 and 16.0 Hz, F-25a); −106.17 (dt, J_{FF} = 258 Hz, J_{FH} = 16.9 Hz, F-25b); HRMS-ESI: calculated for $C_{28}H_{44}F_2NaO_3$: 489.3150, found 489.3170.

*2.1.4. 25,25-Difluoro-3β-hydroxy-27-norcholest-5-en-26-oic acid (**4**)*

To a solution of ester **9** (30.0 mg, 0.0600 mmol) in methanol (1 mL) and THF (1 mL), 5% aqueous LiOH (0.3 mL, 0.700 mmol) was added. The reaction mixture was stirred for 30 min at 25 °C, diluted with water and concentrated to a third of its volume. The mixture was acidified to pH 3 with 1 N HCl and extracted with ethyl acetate. The organic layer was washed with water, dried with sodium sulphate and the solvent evaporated under vacuum. Purification by MPLC RP-18 (flow rate: 5 mL/min; MeOH-H_2O 70:30) gave acid **4** as an amorphous solid (17.0 mg, 60.3%). ^{1}H NMR (500.13 MHz, DMSO-d_6) δ_H: 5.25 (1H, bs, H-6); 3.25 (1H, m, H-3); 2.10 (2H, m, H-4); 1.96 (2H, m, H-24); 1.94 (1H, m, H-12β); 1.90 (1H, m, H-7β); 1.76 (1H, m, H-1β); 1.75 (1H, m, H-16α); 1.66 (1H, m, H-2α); 1.53 (1H, m, H-15β); 1.41 (1H, m, H-23a); 1.50 (1H, m, H-7α); 1.42 (2H, m, H-11); 1.38 (2H, m, H-8 and H-22a); 1.35 (2H, m, H-2β and H-20); 1.25 (1H, m, H-23b); 1.23 (1H, m, H-16β); 1.13 (1H, m, H-12α); 1.04 (1H, m, H-17); 1.06 (1H, m, H-22b); 1.02 (1H, m, H-15α); 0.97 (1H, m, H-1α); 0.96 (1H, m, H-14); 0.93 (3H, s, H-19); 0.88 (3H, d, J = 6.5 Hz, H-21); 0.87 (1H, m, H-9); 0.64 (3H, s, H-18); ^{13}C NMR (125.77 MHz, DMSO-d_6) δ_C: 165.9 (t, J = 30.8 Hz, C-26); 141.7 (C-5); 120.9 (C-6); 117.5 (t, J = 249 Hz, C-25); 70.5 (C-3); 56.7 (C-14); 55.9 (C-17); 50.1 (C-9); 42.7 (C-4); 42.3 (C-13); 39.7 (C-12); 37.4 (C-1); 36.5 (C-10); 35.4 (C-20); 35.3 (C-22); 34.7 (t, J = 23.0, C-24); 31.94 (C-8); 31.89 (C-7); 31.82 (C-2); 28.2 (C-16); 24.3 (C-15); 21.1 (C-11); 19.6 (C-19); 18.8 (C-21); 18.3 (t, J = 3.7, C-23); 12.1 (C-18); ^{19}F NMR (470.59 MHz, DMSO-d_6) δ_F: −106.17 (dt, J_{FF} = 259 Hz, J_{FH} = 18.8 Hz, F-25a); −106.80 (dt, J_{FF} = 259 Hz, J_{FH} = 14.1 Hz, F-25b); HRMS-ESI: calculated for $C_{26}H_{40}F_2NaO_3$: 461.2838, found 461.2833.

*2.1.5. 25,25-Difluoro-27-norcholest-5-ene-3β,26-diol (**5**)*

To a solution of compound **8** (36.0 mg, 0.0600 mmol) in dry THF (7.0 mL) lithium aluminium hydride (4.7 mg, 0.120 mmol) was added under an argon atmosphere. The reaction mixture was stirred 60 min at 25 °C and ethyl acetate (10 mL) added. The mixture was percolated through a celite plug and the solvent evaporated to give alcohol **10** as an amorphous solid (32.1 mg). Compound **10** was treated with HF-AcN following the procedure previously described for **9**. Purification of the resulting solid by MPLC (Flow rate: 10 mL/min; hexane-ethyl acetate 70:30) gave the 26-hydroxysteroid **5** as an amorphous solid (20.0 mg, 75.0% from **8**). ^{1}H NMR (500.13 MHz, DMSO-d_6) δ_H: 5.27 (1H, bs, H-6); 3.55 (2H, t, J = 13 Hz, H-26); 3.26 (1H, m, H-3); 2.12 (2H, m, H-4); 1.81 (2H, m, H-24); 1.97 (1H, m, H-12β); 1.91 (1H, m, H-7β); 1.77 (1H, m, H-1β); 1.80 (1H, m, H-16α); 1.67 (1H, m, H-2α); 1.55 (1H, m, H-15β); 1.47 (1H, m, H-23a); 1.50 (1H, m, H-7α); 1.45 (2H, m, H-11); 1.46 (2H, m, H-8); 1.38 (1H, m, H-22a); 1.38 (2H, m, H-2β); 0.95(1H, m, H-20); 1.29 (1H, m, H-23b); 1.26 (1H, m, H-16β); 1.15 (1H, m, H-12α); 1.09 (3H, m, H-17); 1.05 (1H, m, H-22b); 1.06 (1H, m, H-15α); 0.98 (1H,

m, H-1α); 0.99 (1H, m, H-14); 0.95 (1H, s, H-19); 0.91 (3H, d, J = 6.5 Hz, H-21); 0.88 (1H, m, H-9); 0.66 (3H, s, H-18); ^{13}C NMR (125.77 MHz, DMSO-d_6) δ_C: 141.7 (C-5); 124.8 (t, J = 241 Hz, C-25); 120.9 (C-6); 70.5 (C-3); 62.6 (t, J = 31.0 Hz, C-26); 56.7 (C-14); 55.9 (C-17); 50.1 (C-9); 42.7 (C-4); 42.3 (C-13); 39.7 (C-12); 37.4 (C-1); 36.5 (C-10); 35.7 (C-22); 35.5 (C-20); 33.5 (t, J = 24.0, C-24); 31.94 (C-8); 31.89 (C-7); 31.83 (C-2); 28.2 (C-16); 24.3 (C-15); 21.1 (C-11); 19.6 (C-19); 18.9 (C-21); 18.4 (t, J = 4.2, C-23); 12.1 (C-18); ^{19}F NMR (470.59 MHz, DMSO-d_6) δ_F: −105.38 (dt, J_{FF} = 242.3 Hz, J_{FH} = 14.7 F-25a); −106.21 (dt, J_{FF} = 242.3 J_{FH} = 14.7 Hz, F-25b); HRMS-ESI: calculated for $C_{26}H_{42}F_2NaO_2$: 447.3045, found 447.3026.

2.2. Biological activity

HEK–293 T cells were cultured at 37 °C under 5% CO_2 humidified atmosphere in DMEM supplemented with 10% fetal calf serum (FCS) containing penicillin (100 IU/mL), streptomycin (100 mg/mL) and glutamine (2 mM) in p100 plates. For transient transfections, 3×10^5 cells were plated in 12-wells plates and transfected with lipofectamine according to the manufacturer protocol (Lipofectamine 2000, Invitrogen). Analyses of human LXRβ or human LXRα activities were performed by transfecting 0.7 μg of the reporter construct pLRE-LUC, 0.6 μg of the respective pLXRβ or pLXRα expression vectors (kindly provided by Dr. Shutsung Liao, University of Chicago), 0.2 μg of human pRXR and 0.6 μg of pRSV-LacZ (Clontech Inc., Palo Alto, CA) as control of transfection. After transfection, the medium was replaced by serum-free medium containing antibiotics. Cells were then incubated during 18 h with GW3965 (Sigma), compound **4** or compound **5** at the concentrations indicated. Ligands were applied from 1000-fold stock solutions in dimethylsulfoxide (DMSO). Incubations were stopped by aspirating the medium and washing the cells twice with phosphate buffered saline solution (PBS). Cells were then harvested in lysis buffer and luciferase activity was measured according to the manufacturer protocol (Promega Inc.). Galactosidase activity was measured as previously described [8]. Statistical analyses were performed with STATISTICA 6.0 (StatSoft Inc.) and consisted in one-way ANOVA followed by Tukey's multiple comparisons tests. Differences were regarded as significant at $p < 0.05$.

2.3. Computational methods

2.3.1. Initial structures of LXRβ/ligand complexes

The starting coordinates of the LXRβ ligand binding domain was taken from the crystal structure of the LXRβ/24S,25-epoxycholesterol complex (pdb:1p8d, chain A). The missing residues of the H1-H3 loop (255–258) were added with the Modeller program [9]. The LXRβ/GW3965 complex was constructed by superimposing the protein backbone with the protein backbone of pdb:4nqa, and extracting the GW3965 coordinates. In order to build the LXRβ/**4** and LXRβ/**5** complexes, the HF/6-31G** optimized structures of the steroids were introduced by superimposing the skeleton carbon atoms with the corresponding atoms of 24S,25-epoxycholesterol. For the force field parameters of the ligands, RESP (restraint electrostatic potential) atomic partial charges were computed using the HF/6-31G** method in the quantum chemistry program Gaussian 09 [10] for the corresponding optimized structures.

2.3.2. Molecular dynamics

Molecular dynamics (MD) were performed with the AMBER 14 software package [11]. Ligand parameters were assigned according to the general AMBER force field (GAFF) and the corresponding RESP charges using the Antechamber (See Tables S1, S2 and S3). The FF14SB force field parameters were used for all receptor residues. Complexes were immersed in an octahedral box of TIP3 P water molecules using the Tleap module, giving final systems of around 30000 atoms. Systems were initially optimized and then gradually heated to a final temperature of 300 K. Starting from these equilibrated structures, MD production runs of 400 ns were performed. All simulations were performed at 1 atm and 300 K, maintained with the Berendsen barostat and thermostat respectively, using periodic boundary conditions and the particle mesh Ewald method (grid spacing of 1 Å) for treating long-range electrostatic interactions with a uniform neutralizing plasma. The SHAKE algorithm was used to keep bonds involving H atoms at their equilibrium length, allowing the use of a 2 fs time step for the integration of Newton's equations.

2.3.3. Analysis of results

The root mean squared deviation (RMSD) of backbone receptor atoms, ligand atoms or side chain atoms of His435 and Trp457; the root mean square fluctuations (RMSF) of CA receptor residues; the time evolution of the distances among selected atoms, and the time evolution of torsion angles between selected atoms were monitored with the CPPTRAJ module [12]. The temporal evolution of the secondary structural propensity for the H11-H12 region was evaluated by the DSSP method [13] implemented in the CPPTRAJ module. Trajectories were visualized and representative snapshots were obtained using VMD [14]. The MM/PBSA.py tool [15]

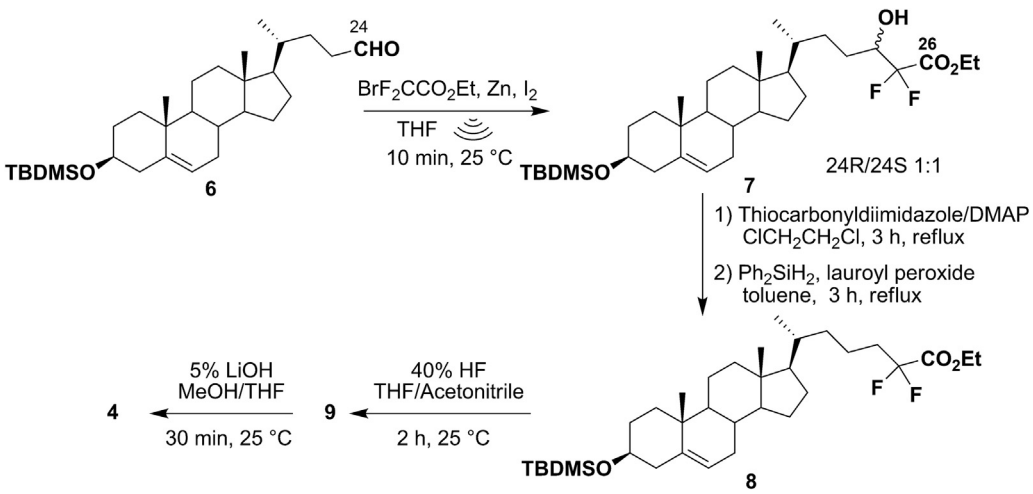

Scheme 1. Synthesis of 25,25-difluoro 3β-hydroxy-27-norcholest-5-en-26-oic acid (**4**).

implemented in AMBER was used to compute the electrostatic (ele) and Van der Waals (vdw) contributions to the total energy of the molecular mechanics (MM) force field in the gas phase. Calculations were performed over 6000 snapshots of the last 300 ns of the trajectory, previous deletion of water molecules.

3. Results and discussion

3.1. Chemistry

Compound **4** was obtained from compound **6** [16], as depicted in Scheme 1. A Reformatsky reaction on the C-24 aldehyde with ethyl bromodifluoroacetate, was used to introduce the difluoromethylene group. Preliminary attempts to carry out this reaction in THF under reflux were unsuccessful (Table 1, entries 1 and 2). Ultrasonic irradiation has been used as an alternative for reactions ordinarily accomplished by heating, being especially useful for heterogeneous systems where metals are involved. Hans and Boudjouk reported that the use of a low-intensity ultrasonic laboratory cleaning bath greatly improved the yields of Reformatsky reactions of simple aldehydes and ketones with ethyl bromoacetate [17], while high intensity ultrasound (HIU) has been used to promote Reformatsky reactions of phenyl ketones and α-bromoesters [18]. Based on these reports, we tried different experimental conditions for the condensation of aldehyde **6** with ethyl bromodifluoroacetate under HIU irradiation (Table 1). Compound **7** was obtained in 50% yield as a 1:1 mixture of epimers at C-24, using 3 equivalents of Zn and 3 equivalents of ethyl bromodifluoroacetate, a catalytic amount of iodine and THF as solvent (entry 3). Increasing the number of equivalents or the reaction time did not improve the reaction yield (entries 4, 5). The use of chlorotrimethylsilane as an additive in Reformastky reactions has been reported to activate the formation of the intermediate organozincate [19], however in our case it led to the generation of undesired byproducts (entry 6). Previously it was established that the Reformastky reactions under HIU was concentration dependent [18], in our case lowering the amount of solvent improved the reaction yield to 65% (entry 7). No significant changes were observed when toluene was used as solvent (entry 8). The 24-hydroxyl in **7** was removed by a Barton-McCombie deoxygenation using thiocarbonyldiimidazole and dimethylaminopyridine to generate the corresponding thionocarbonate, followed by treatment with diphenylsilane and lauroyl peroxide to give compound **8** (73% yield from **7**) [20]. Removal of the silyl protecting group at C-3 (40% hydrofluoric acid) gave compound **9**. Treatment of **9** with lithium hydroxide in THF-methanol-water gave the difluoro-27-norcholestenoic acid **4** (57% from **8**). The 26-alcohol **5** was prepared from **8** by reduction of the C-26 ester ($LiAlH_4$/THF), followed by cleavage of the silyl ether with 40% hydrofluoric acid (75% from **8**, Scheme 2).

Table 1
Reformatsky reaction on aldehyde **6**.

Entry	Zn (wt%)	[**6**] (M)	Additives	**6**/$BrCF_2CO_2Et$/Zn	Conditions	% **7**[a]
1	0.39	0.02	I_2 (cat)	1:2:3	Reflux, 1 h	–
2	0.39	0.02	TMSCl (6 eq)	1:2:3	Reflux, 1 h	–
3	1.25	0.06	I_2 (cat)	1:3:3	HIU, 10 min	50%
4	1.6	0.06	I_2 (cat)	1:4:4	HIU, 10 min	53%
5	1.6	0.06	I_2 (cat)	1:4:4	HIU, 20 min	45%
6	1.6	0.06	TMSCl (6 eq)	1:4:4	HIU, 10 min	35%
7	4	0.21	I_2 (cat)	1:3:3	HIU, 10 min	65%
8[b]	4	0.21	I_2 (cat)	1:3:3	HIU, 10 min	62%

THF was used as solvent except where noted. HIU: High intensity ultrasound irradiation.
[a] Isolated yield.
[b] Toluene was used as solvent.

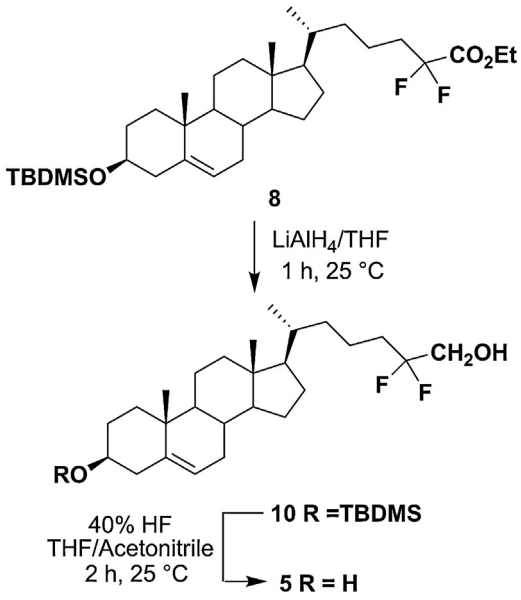

Scheme 2. Synthesis of 25,25-difluoro-27-norcholest-5-ene-3β,26-diol (**5**).

3.2. Biological activity

The biological activity of compounds **4** and **5** was determined by a luciferase reporter assay in the human HEK293 T cells co-transfected with full length human LXRβ expression vector (Fig. 2). The difluoroacid **4** significantly reduced basal levels of luciferase activity, behaving as an inverse agonist, similar to the 27-norcholestenoic acid **3** [7]. Moreover, when compound **4** was co-administered together with GW3965, a marked inhibitory effect was observed. Similar results were obtained when we assessed the full length human LXRα activity (Fig. S1). Therefore, the introduction of two fluorine atoms at C-25 did not affect the activity profile. On the other hand the difluoroalcohol **5** *per se*, showed agonist activity and did not inhibit the effect of the synthetic LXR agonist GW3965. Thus the increased acidity of the 26-alcohol due to the neighboring fluorine atoms, would not be enough for the 27-nor side chain to confer antagonist or inverse agonist properties. Together, the reporter gene assays revealed that

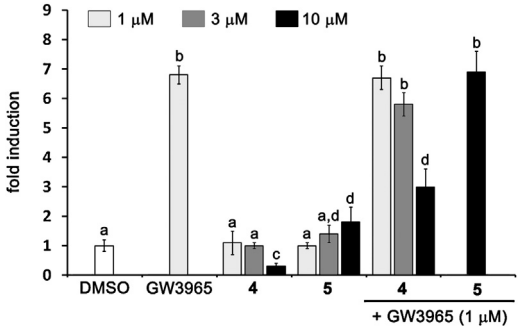

Fig. 2. Biological activity of compounds **4** and **5**. HEK–293 T cells were cotransfected with pLRE-LUC, pRXR and pLXRβ vectors and then incubated for 18 h as indicated. Luciferase activity was measured and normalized with β-galactosidase activity. Values are expressed as fold induction relative to the control (DMSO). Means ± S.E. from three independent experiments are shown. Differences were determined by one-way ANOVA followed by Tukey's multiple comparisons tests. Bars with different superscript letters are significantly different from each other ($p < 0.05$).

both fluorinated analogues conserved the ability to modulate LXRβ activity, although in opposing ways.

3.3. Molecular dynamics simulation of LXR/ligand complexes

In order to investigate the molecular basis of the interaction between the LXRβ and the fluorinated analogues **4** and **5**, we carried out 400 ns molecular dynamics (MD) simulations of the LXRβ/**4** and the LXRβ/**5** complexes. The LXRβ/GW3965 MD simulation was also ran as a control trajectory. All complexes were constructed from the crystal structure of the LXRβ/24S,25-epoxycholesterol complex, using a similar procedure to that used previously to construct the LXRβ LBD/**1** and LXRβ LBD/**3** complexes [7]. In the case of the non-steroidal agonist GW3965, the ligand coordinates of the pdb:4nqa structure were used.

3.3.1. Global analysis of receptor structures

We started our analysis by verifying the stability of the LXRβ/ligand systems along the 400 ns MD runs. Visual inspection showed that the global folding remained essentially intact, and the time-dependent residue fluctuation (root-mean square deviations, RMSD) measured over the backbone atoms from the initial structures revealed that all simulations were reasonably stable (Fig. S2a). The average RMSD for GW3965, difluoroacid **4** and difluoroalcohol **5** systems(Table 2), suggest that the receptor undergoes more conformational changes in the presence of the difluoroacid **4**.

To study the dynamical behavior of the protein backbone, we calculated the RMSF (root-mean square fluctuations) in the three LXRβ/ligand systems, that provides a time-average representation of per-residue fluctuations. Fig. 3 shows that all systems displayed a similar global fluctuation pattern. However, a detailed comparison among systems revealed that the difluoroacid **4** produced a significant alteration in the C-terminal region of the H11 helix and in the H11-H12 loop (from Ser432 to Pro450). In the GW3965 and difluoroalcohol **5** systems, the Ser432 to Leu444 region showed small RMSF values, which agree with a well-structured α-helix, while the H11-H12 loop residues (Asp445 to Pro450) presented a larger fluctuation. In contrast, a marked increase in the mobility of the Ser432 to Leu444 region occurs when the inverse agonist **4** is bound, concomitantly with a small fluctuation of loop residues.

Given these results, we used the DSSP method [13] to calculate the temporal evolution of the secondary structural propensity for the H11-H12 region (Fig. S3). Significant changes were obtained in the C-terminal region of H11 for the LXRβ/**4** system. These residues, which form a stable α-helix in GW3965 and in compound **5** complexes, shift to another structural motif, such as 3–10 helix and turn, or completely lose the secondary structure after the first 100 ns of simulation. Fig. 4 shows the superposition of representative snapshots of either LXRβ/**4** or LXRβ/**5** complexes and the LXRβ/GW3965 system, where a notorious deformation of the C-terminal H11 residues can be observed in the former. Thus, the global analysis of the receptor structures revealed that the difluoroacid **4** induces a different dynamic behavior on the LXRβ compared to agonists GW3965 and difluoroalcohol **5**.

Table 2
Thermodynamical and structural information of LXRβ complexes with GW3965, and compounds **4** and **5**.

	GW3965	**4**	**5**
Average RMSD (Å)[a]			
Receptor	1.5	1.7	1.5
Ligand	0.6	1.0	0.9
MM (kcal/mol)[b]			
vdw	−75.5	−59.7	−60.1
ele	−37.1	−12.1	−14.4
MM	−112.6	−71.8	−74.5

[a] Average RMSD values measured over receptor backbone or ligand heavy atoms.
[b] Interaction energy contributions to the total energy of the MM force field in the gas phase computed using the MM/PBSA method (vdw: Van der Waals; ele: electrostatic; MM: total gas phase binding energy).

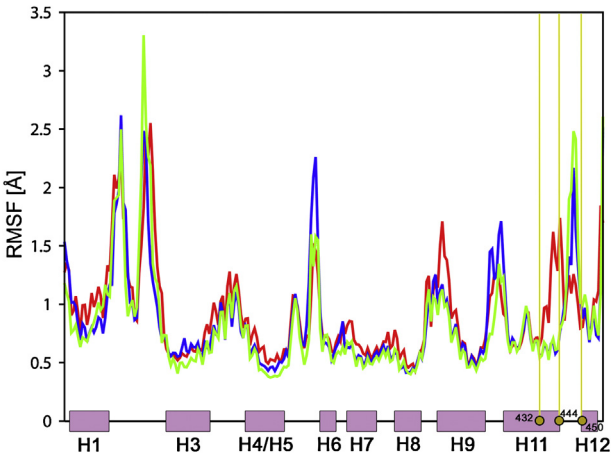

Fig. 3. RMSF values of the LXRβ/GW3965 (green), LXRβ/**4** (red) and LXRβ/**5** (blue) complexes. The secondary structure of LXRβ LBD is schematized along the x-axis. (For interpretation of the references to colour in this figure legend, the reader is referred to the web version of this article.)

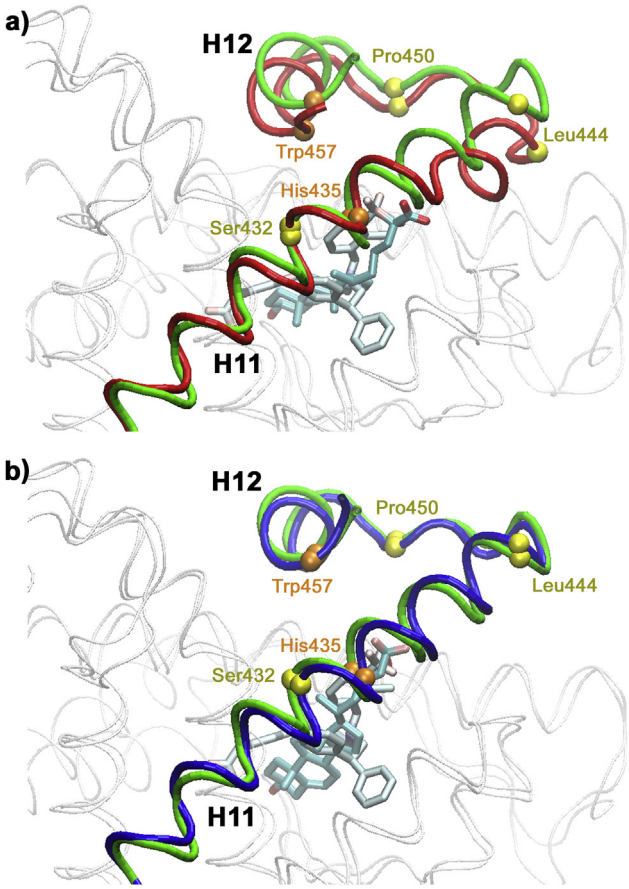

Fig. 4. Superposition of representative snapshots of a) LXRβ/GW3965 (green) and LXRβ/**4** (red), b) LXRβ/GW3965 (green) and LXRβ/**5** (blue), showing the H11-H12 region. CA atoms of relevant residues are shown as yellow balls (Ser432, Leu444 and Pro450) or orange balls (His435 and Trp457). (For interpretation of the references to colour in this figure legend, the reader is referred to the web version of this article.)

3.3.2. Ligand binding mode and activation mechanism

Visual inspection of the MD trajectories revealed that the global orientation of all ligands was conserved along the simulation timescale. Remarkably, although the initial LXRβ LBD structure used to build these systems comes from a steroidal complex, GW3965 was the ligand which exhibited the smallest positional modifications (Fig. S2b). Compounds **4** and **5** had larger RMSD values, mainly due to variations in the position of the steroid side chain. In order to obtain an estimation of the ligand-receptor interaction in each MD trajectory, the MM/PBSA method was used to compute the energetic contributions from the electrostatic energy and Van der Waals interactions [15]. We found that GW3965 had the most favorable binding mode, while it was less favorable and similar for compounds **4** and **5** (Table 2). Although the Van der Waals term was the major contributor in all cases, its relative importance was higher for both steroidal ligands.

As mentioned in Section 1, the crystal structures of LXRβ/GW3965 complex show that the trifluoromethyl moiety of the ligand interacts with His435. Our simulation showed that not only the orientation of the trifluoromethyl group is conserved, but actually a stable (NE2)-H-F hydrogen bond exists (Fig. 5a). Frequencies are similar for the three fluorine atoms (Fig. S4a), indicating a free rotation of the trifluoromethyl group. The MD simulation also showed that, except for His435, the fluorine atoms are always surrounded by non-polar residues in helices H3, H7 and H11 and in the H6-H7 and H11-H12 loops (Fig. S5). The aromatic–aromatic interaction of the His435 and Trp457 residues, located in helix 11 and at the end of helix 12 respectively, has been associated with LXRβ activation [21]. The RMSD curve for the LXRβ/GW3965 complex simulation showed that those essential residues remained positioned in their original coordinates along the whole simulation (Figs. 6a and 6b, respectively), indicating a well established aromatic–aromatic interaction (Fig. 5a) that would be crucial for the receptor to acquire a stable agonist conformation.

In the case of compound **5**, the 26-hydroxyl moiety and both fluorine atoms alternate their interaction with the His435 residue (Fig. 5c and Fig. S4b). Remarkably, the fluorine atoms in compound **5** occupied a position similar to that of the fluorine atoms in GW3965, contacting the same non polar residues (Fig. S5). Moreover, the LXRβ/**5** complex also maintained a stable agonist conformation, similar to that of LXRβ/GW3965, with small RMSD values for the His435 and slightly larger for the Trp457 (Figs. 6a and 6b, respectively), but without altering the original aromatic–aromatic interaction between these residues.

The ligand binding mode of compound **4** showed larger differences compared to the above agonist systems. The interaction between the ligand and His435 occurs mainly through the carboxylate group, while the participation of the fluorine atoms is minimal (Fig. 5b and Fig. S4c). Although this leads to moderate changes on the His435 residue (Fig. 6a), the major change was observed in the conformation of Trp457 (Fig. 6b). In fact, a pronounced destabilization of the original position during the first part of the trajectory followed by an abrupt conformational change was observed by monitoring the temporal evolution of the Trp457 χ2 angle (CA-CB-CG-CD1) (Fig. 6c). The Trp457 side chain rotated in a way that exposed the indole nitrogen atom (NE1 atom) to the

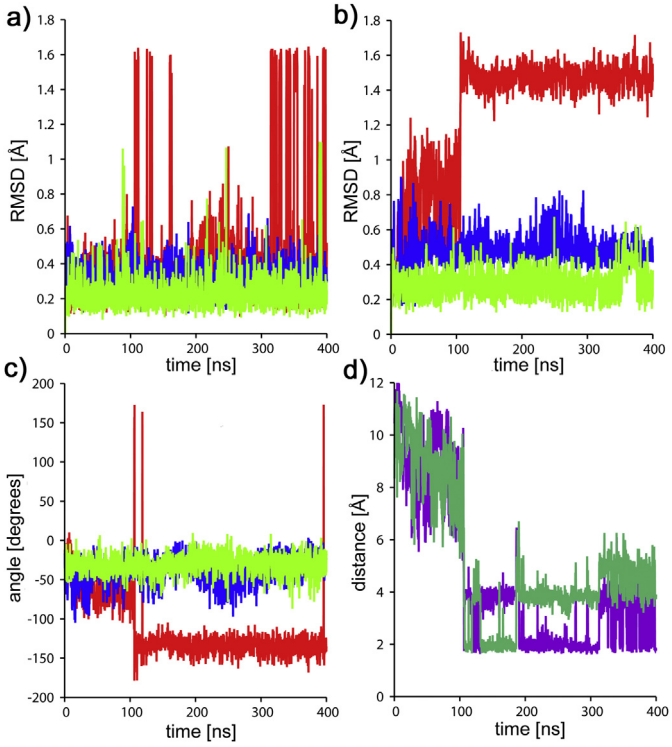

Fig. 6. RMSD of the initial structures measured over side chain atoms of a) His435 or b) Trp457 and c) time evolution of the χ2 torsion angle CA-CB-CG-CD of Trp457, in LXRβ/GW3965 (green), LXRβ/**4** (red) and LXRβ/**5** (blue) complexes. d) Time evolution of the distance between the NE1 atom of Trp457 and the oxygen atoms of the carboxylate group of difluoroacid **4** in the LXRβ/**4** complex. (For interpretation of the references to colour in this figure legend, the reader is referred to the web version of this article.)

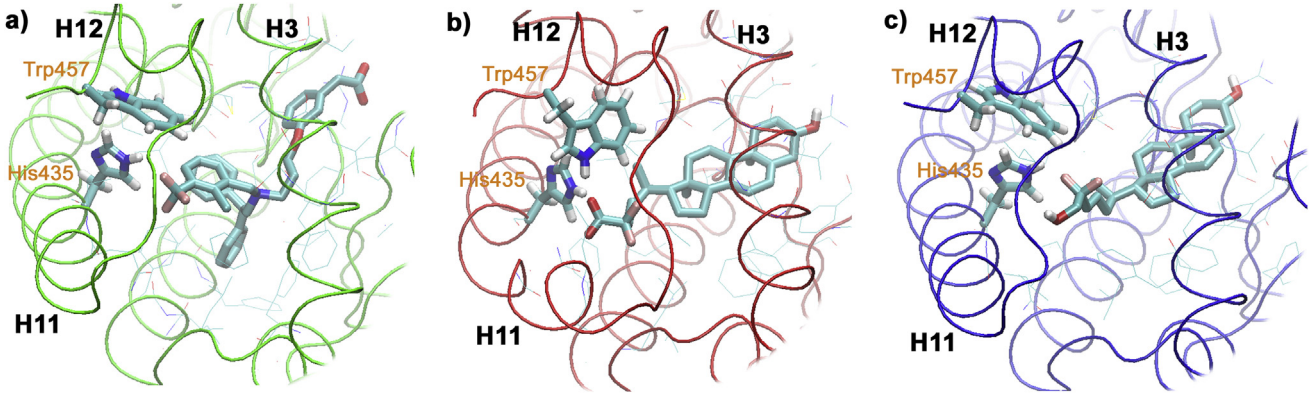

Fig. 5. Representative snapshots of the ligand binding mode of a) GW3965, b) difluoroacid **4** and c) difluoroalcohol **5**.

ligand carboxylate group, forming a strong hydrogen bond that remained stable during the rest of the simulation (Fig. 6d). As a measurement of the disturbance that this phenomenon produced in the His435-Trp457 aromatic–aromatic interaction, we calculated the temporal evolution of the distance between their centers of mass. We found that the presence of compound **4** increased the average separation between these residues in 0.5 Å (4.9 Å for GW3965 and compound **5**, and 5.4 Å for compound **4**). Together these results support the idea that the inverse agonist compound **4** produces a substantial destabilization of the agonist arrangement.

4. Conclusion

The wide tissue distribution of compounds **1** and **2**, together with their ability to modulate the gene expression through the LXRs, make these metabolites very important components of cellular signalling. As members of the NR superfamily, the central mechanism of LXRs activation comprises the overall shape of the AF-2 region, which is mainly determined by the conformation of the H12 helix. In particular, two residues play a crucial role in the molecular mechanism of LXRs action: the His435 at H11 and the Trp457 at H12 helices. Both steroidal and non steroidal ligands interact with His435, constraining its position and allowing a T-shaped aromatic–aromatic interaction with the Trp457 [22,23]. In this way, by interacting with the His435, agonist ligands indirectly promote the orientation of Trp457 to maintain the H12 in an agonistic state.

The fluorinated oxysterols **4** and **5** allow us to further investigate how small modifications of the steroid side chain may induce conformational changes in the AF-2 domain of the receptor, that could affect the final LXR biochemistry [7,24]. In the case of the synthetic inverse agonist **3**, introduction of the fluorine atoms at C-25 had a negligible effect on its LXR activity in the reporter gene assay. However MD simulations showed that the effect of compound **4** on the His435-Trp457 aromatic–aromatic interaction and the resulting conformational changes on the H11-H12 region of LXRβ, differ from those induced by its non-fluorinated analogue **3** [7] and thus may lead to subtle differences in coactivator/corepressor recruiting. Based on the similar activities of the natural ligands **1** and **2** [1], the difluoroalcohol **5** was initially proposed as a less acidic analogue of **4**. However in this case as shown by the MD simulation, the fluorine atoms actively participate in the interaction with several residues in the ligand binding pocket leading to a stabilization of the active receptor conformation. This was confirmed by the agonistic activity observed in the reporter gene assay. Our results thus suggest that the negatively charged carboxylate in **3** and **4** is required to disrupt the His435-Trp457 aromatic–aromatic interaction and give rise to the inverse agonist activity.

Supplementary material

Figures S1-S5, ^{1}H and ^{13}C NMR spectra of compounds **4**, **5**, **7**, **8** and **9**, GAFF atom types and RESP atomic partial charges for ligands (Tables S1-S3) and .mol files of the initial optimized ligand geometries. Supplementary data associated with this article can be found, in the online version.

Acknowledgements

This work was supported by grants from Agencia Nacional de Promoción Científica y Tecnológica (PICT 2010-0623), CONICET-Argentina (PIP 11220110100702 and PIP11420080100567) and Universidad de Buenos Aires (N° 20020100100281).

Appendix A. Supplementary data

Supplementary data associated with this article can be found, in the online version, at http://dx.doi.org/10.1016/j.jsbmb.2016.07.001.

References

[1] C. Song, S. Liao, Cholestenoic acid is a naturally occurring ligand for liver x receptor α, Endocrinology 141 (2000) 4180–4184.
[2] E.R. Nelson, S.E. Wardell, J.S. Jasper, S. Park, S. Suchindran, M.K. Howe, N.J. Carver, R.V. Pillai, P.M. Sullivan, V. Sondhi, M. Umetani, J. Geradts, D.P. McDonnell, 27-Hydroxycholesterol links hypercholesterolemia and breast cancer pathophysiology, Science 342 (2013) 1094–1098.
[3] C. Huang, Natural modulators of liver X receptors, J. Integr. Med. 12 (2014) 76–85.
[4] P. Xu, D. Li, X. Tang, X. Bao, J. Huang, Y. Tang, Y. Yang, H. Xu, X. Fan, LXR agonists: new potential therapeutic drug for neurodegenerative diseases, Mol. Neurobiol. 48 (2013) 715–728.
[5] X. Jiao, D.J. Kopecky, B. Fisher, D.E. Piper, M. Labelle, S. McKendry, M. Harrison, S. Jones, J. Jaen, A.K. Shiau, P. Escaron, J. Danao, A. Chai, P. Coward, F. Kayser, Discovery and optimization of a series of liver X receptor antagonists, Bioorg. Med. Chem. Lett. 22 (2012) 5966–5970.
[6] C.A. Flaveny, K. Griffett, D. El-Gendy Bel, M. Kazantzis, M. Sengupta, A.L. Amelio, A. Chatterjee, J. Walker, L.A. Solt, T.M. Kamenecka, T.P. Burris, Broad anti-tumor activity of a small molecule that selectively targets the warburg effect and lipogenesis, Cancer Cell 28 (1) (2015) 42–56.
[7] L.D. Alvarez, M.V. Dansey, D.Y. Grinman, D. Navalesi, G.A. Samaja, M.C. del Fueyo, N. Bastiaensen, R. Houtman, D.A. Estrin, A.S. Veleiro, A. Pecci, G. Burton, Destabilization of the torsioned conformation of a ligand side chain inverts the LXRβ activity, Biochim. Biophys. Acta Mol. Cell Biol. Lip. 1851 (2015) 1577–1586.
[8] A. Veleiro, M.C. Pecci, R. Monteserin, M.T. Baggio, C.P. Garland, G. Lantos, 6,19-Sulfur-bridged progesterone analogues with antiimmunosuppressive activity, J. Med. Chem. 48 (2005) 5675–5683.
[9] A. Sali, T.L. Blundell, Comparative protein modelling by satisfaction of spatial restraints, J. Mol. Biol. 234 (1993) 779–815.
[10] M.J. Frisch, G.W. Trucks, H.B. Schlegel, G.E. Scuseria, M.A. Robb, J.R. Cheeseman, G. Scalmani, V. Barone, B. Mennucci, G.A. Petersson, H. Nakatsuji, M. Caricato, X. Li, H.P. Hratchian, A.F. Izmaylov, J. Bloino, G. Zheng, J.L. Sonnenberg, M. Hada, M. Ehara, K. Toyota, R. Fukuda, J. Hasegawa, M. Ishida, T. Nakajima, Y. Honda, O. Kitao, H. Nakai, T. Vreven, J.A. Montgomery Jr., J.E. Peralta, F. Ogliaro, M.J. Bearpark, J. Heyd, E.N. Brothers, K.N. Kudin, V.N. Staroverov, R. Kobayashi, J. Normand, K. Raghavachari, A.P. Rendell, J.C. Burant, S.S. Iyengar, J. Tomasi, M. Cossi, N. Rega, N.J. Millam, M. Klene, J.E. Knox, J.B. Cross, V. Bakken, C. Adamo, J. Jaramillo, R. Gomperts, R.E. Stratmann, O. Yazyev, A.J. Austin, R. Cammi, C. Pomelli, J.W. Ochterski, R.L. Martin, K. Morokuma, V.G. Zakrzewski, G.A. Voth, P. Salvador, J.J. Dannenberg, S. Dapprich, A.D. Daniels, Ö. Farkas, J.B. Foresman, J.V. Ortiz, J. Cioslowski, D.J. Fox, Gaussian 09, Gaussian, Inc, Wallingford, CT, USA, 2009.
[11] J.T.B.D.A. Case, R.M. Betz, D.S. Cerutti, T.E. Cheatham III, T.A. Darden, R.E. Duke, T.J. Giese, H. Gohlke, A.W. Goetz, N. Homeyer, S. Izadi, P. Janowski, J. Kaus, A. Kovalenko, T.S. Lee, S. LeGrand, P. Li, T. Luchko, R. Luo, B. Madej, K.M. Merz, G. Monard, P. Needham, H. Nguyen, H.T. Nguyen, I. Omelyan, A. Onufriev, D.R. Roe, A. Roitberg, R. Salomon-Ferrer, C.L. Simmerling, W. Smith, J. Swails, R.C. Walker, J. Wang, R.M. Wolf, X. Wu, D.M. York, P.A. Kollman, Amber 15, University of California, San Francisco, 2015.
[12] D.R. Roe, T.E. Cheatham, 3rd, PTRAJ and CPPTRAJ: Software for processing and analysis of molecular dynamics trajectory data, J. Chem. Theory Comput. 9 (2013) 3084–3095.
[13] W. Kabsch, C. Sander, Dictionary of protein secondary structure: pattern recognition of hydrogen-bonded and geometrical features, Biopolymers 22 (1983) 2577–2637.
[14] W. Humphrey, A. Dalke, K. Schulten, VMD: visual molecular dynamics, J. Mol. Graphics 14 (1) (1996) 33–38, 27–38.
[15] B.R. Miller 3rd, T.D. McGee Jr., J.M. Swails, N. Homeyer, H. Gohlke, A.E. Roitberg, MMPBSA. py: an efficient program for end-state free energy calculations, J. Chem. Theory Comput. 8 (2012) 3314–3321.
[16] M.V. Dansey, L.D. Alvarez, G. Samaja, D.S. Escudero, A.S. Veleiro, A. Pecci, O.A. Castro, G. Burton, Synthetic DAF-12 modulators with potential use in controlling the nematode life cycle, Biochem. J. 465 (2015) 175–184.
[17] B.H. Han, P. Boudjouk, Organic sonochemistry. Sonic acceleration of the Reformatsky reaction, J. Org. Chem. 47 (1982) 5030–5032.
[18] N.A. Ross, R.A. Bartsch, High-intensity ultrasound-promoted Reformatsky reactions, J. Org. Chem. 68 (2003) 360–366.
[19] B. Hatano, K. Nagahashi, T. Kijima, Zinc-mediated allylation and alkylation of aminals in the presence of TMSCl and diisopropylamine, J. Org. Chem. 73 (2008) 9188–9191.
[20] D.H.R. Barton, D.O. Jang, J.C. Jaszberenyi, The invention of radical reactions. Part XXXI. Diphenylsilane: a reagent for deoxygenation of alcohols via their thiocarbonyl derivatives, deamination via isonitriles, and dehalogenation of bromo- and iodo- compounds by radical chain chemistry, Tetrahedron 49 (1993) 7193–7214.

[21] S. Williams, R.K. Bledsoe, J.L. Collins, S. Boggs, M.H. Lambert, A.B. Miller, J. Moore, D.D. McKee, L. Moore, J. Nichols, D. Parks, M. Watson, B. Wisely, T.M. Willson, X-ray crystal structure of the liver X receptor beta ligand binding domain: regulation by a histidine-tryptophan switch, J. Biol. Chem. 278 (2003) 27138–27143.
[22] A. Chawla, J.J. Repa, R.M. Evans, D.J. Mangelsdorf, Nuclear receptors and lipid physiology: opening the X-files, Science 294 (2001) 1866–1870.
[23] N. Malini, H. Rajesh, P. Berwal, S. Phukan, V.N. Balaji, Analysis of crystal structures of LXR beta in relation to plasticity of the ligand-binding domain upon ligand binding, Chem. Biol. Drug Des. 71 (2008) 140–154.
[24] M. Albers, B. Blume, T. Schlueter, M.B. Wright, I. Kober, C. Kremoser, U. Deuschle, M. Koegl, A novel principle for partial agonism of liver X receptor ligands. Competitive recruitment of activators and repressors, J. Biol. Chem. 281 (2006) 4920–4930.